

See discussions, stats, and author profiles for this publication at: <https://www.researchgate.net/publication/270716669>

2D Complex Shear Modulus Imaging in Gaussian Noise

Conference Paper in IFMBE proceedings · January 2015

DOI: 10.1007/978-3-319-11776-8_94

READS

47

3 authors:



[Nguyen Thi Anh Dao](#)

University of Technology and Logistics

2 PUBLICATIONS 1 CITATION

SEE PROFILE



[Duc-Tan Tran](#)

Vietnam National University, Hanoi

125 PUBLICATIONS 118 CITATIONS

SEE PROFILE



[Nguyen Linh-Trung](#)

Vietnam National University, Hanoi

51 PUBLICATIONS 379 CITATIONS

SEE PROFILE

Vo Van Toi · Tran Ha Lien Phuong
Editors

5th International Conference on Biomedical Engineering in Vietnam

 Springer

Editors

Vo Van Toi
Biomedical Engineering Department
International University
Vietnam National Universities
Ho Chi Minh City
Vietnam

Tran Ha Lien Phuong
Biomedical Engineering Department
International University
Vietnam National Universities
Ho Chi Minh City
Vietnam

ISSN 1680-0737 ISSN 1433-9277 (electronic)
ISBN 978-3-319-11775-1 ISBN 978-3-319-11776-8 (eBook)
DOI 10.1007/978-3-319-11776-8

Library of Congress Control Number: 2014954484

Springer Cham Heidelberg New York Dordrecht London

© Springer International Publishing Switzerland 2015

This work is subject to copyright. All rights are reserved by the Publisher, whether the whole or part of the material is concerned, specifically the rights of translation, reprinting, reuse of illustrations, recitation, broadcasting, reproduction on microfilms or in any other physical way, and transmission or information storage and retrieval, electronic adaptation, computer software, or by similar or dissimilar methodology now known or hereafter developed. Exempted from this legal reservation are brief excerpts in connection with reviews or scholarly analysis or material supplied specifically for the purpose of being entered and executed on a computer system, for exclusive use by the purchaser of the work. Duplication of this publication or parts thereof is permitted only under the provisions of the Copyright Law of the Publisher's location, in its current version, and permission for use must always be obtained from Springer. Permissions for use may be obtained through RightsLink at the Copyright Clearance Center. Violations are liable to prosecution under the respective Copyright Law.

The use of general descriptive names, registered names, trademarks, service marks, etc. in this publication does not imply, even in the absence of a specific statement, that such names are exempt from the relevant protective laws and regulations and therefore free for general use.

While the advice and information in this book are believed to be true and accurate at the date of publication, neither the authors nor the editors nor the publisher can accept any legal responsibility for any errors or omissions that may be made. The publisher makes no warranty, express or implied, with respect to the material contained herein.

The IFMBE Proceedings is an Official Publication of the International Federation for Medical and Biological Engineering (IFMBE)

Printed on acid-free paper

Springer is part of Springer Science+Business Media (www.springer.com)

Table of Contents

Development of Individual Plasmonic Nanosensors for Clinical Diagnosis <i>Phuoc Long Truong and Sang Jun Sim</i>	1
YALES2BIO: A Computational Fluid Dynamics Software Dedicated to the Prediction of Blood Flows in Biomedical Devices <i>S. Mendez, C. Chnafa, E. Gibaud, J. Sigüenza, V. Moureau, and F. Nicoud</i>	7
Numerical and Experimental Mixing Studies in a Split and Recombine Micromixer with Ellipse-Like Micropillars <i>Nhut Tran-Minh, Erik Andrew Johannessen, and Frank Karlsen</i>	11
Multiplex DNA Biosensor for Viral Infection Diagnosis Using SERS Molecular Sentinel-on-Chip <i>Hoan T. Ngo, Hsin-Neng Wang, Thomas Burke, Christopher Woods, Geoffrey S. Ginsburg, and Tuan Vo-Dinh</i>	15
Whispering Gallery Mode Biosensing – A Detailed Study on ZnO Microspheres <i>Ngo Huynh Buu Trong, Paul Ching-Hang Chien, Yu-Da Chen, Shang-Hsuan Wu, Fu-Chen Hsiao, Linh-Nam Nguyen, and Yia-Chung Chang</i>	21
Ultrasonic Assessment of the Radius <i>J.J. Kaufman, G.M. Luo, F. Rosete, M. Bucovsky, E.M. Stein, E. Shane, and R.S. Siffert</i>	25
High-Resolution Imaging of Dispersive Ultrasonic Guided Waves in Human Long Bones Using Regularized Radon Transforms <i>Tho N.H.T. Tran, Lawrence H. Le, and Mauricio D. Sacchi</i>	28
Adaptive Noise Cancellation in the Intercept Time-Slowness Domain for Eliminating Ultrasonic Crosstalk in a Transducer Array <i>K.C.T. Nguyen, Lawrence H. Le, Mauricio D. Sacchi, L.Q. Huynh, and E. Lou</i>	32
Simulation of Ultrasound Propagation in Long Bone with Depth-Varying Porosity <i>Vu-Hieu Nguyen and Salah Naili</i>	36
Frequency Independence of Ultrasound Transit Time Spectroscopy <i>M.-L. Wille and C.M. Langton</i>	39
<i>In Vitro</i> Ultrasonic Assessment of the Biomechanical Quality of the Interface Surrounding a Dental Implant <i>R. Vayron and G. Haiat</i>	43
Silicon-Based Fabrication of Biodegradable Polymer for Controlled Drug-Delivery <i>Thanh D. Nguyen, Robert S. Langer, and Ana Jaklenec</i>	47
Advancement in Gemcitabine Delivery for Cancer Treatment <i>Uyen Minh Le</i>	51
Multifunctional Drug Nanosystems: A Summary of Recent Researches at IMS/VAST <i>X.P. Nguyen, T.T. TMai, P.T. Ha, H.N. Pham, H.N. Luu, H.M. Do, D.L. Tran, H.N. Nguyen, L.T. Nguyen, A.S. Ho, and T.M.N. Hoang</i>	55
Preparation, Characterization and Antibacterial Curcumin Encapsulated Chitosan-PAA Silver Nanocomposite Films <i>N.V. Cuong, P.N.N. Han, N.K. Hoang, and N.N.L. Giang</i>	58

Investigation of the Synthetic Process of Nano-Hydroxyapatite (Hap) Using Microwave and Ultrasound	332
<i>Tran Thi Tuong Van, Bui Ngoc Thao Tram, Vo Van Toi, and Thi-Hiep Nguyen</i>	
Synthesis and Characterization of Hydroxyapatite Biomaterials from Bio Wastes	336
<i>Bui Ngoc Thao Tram, Thi-Hiep Nguyen, and Vo Van Toi</i>	
Modified DNA Extraction Method for the Detection of <i>Aspergillus Flavus</i> and <i>Aspergillus Parasiticus</i> in Dried Foods	339
<i>Pham Tuong Vi, Huynh Le Thao Trinh, and Nguyen Thi Hue</i>	
DEMM: A Meta-Algorithm to Predict the pKa of Ionizable Amino Acids in Proteins	343
<i>T.B. Nguyen, K.P. Tan, and M.S. Madhusudhan</i>	
A Threshold Algorithm in a Fall Alert System for Elderly People	347
<i>Pham Ty Phu, Nguyen Thanh Hai, and Nguyen Thanh Tam</i>	
Comparative Study on Human A-Glucosidase	351
<i>Q. Ong and L. Le</i>	
Development of Non-Invasion Method for Prognosis and Early Diagnosis of Cervical Cancer in Vietnamese Patients Based on DNA Methylation Specific PCR	355
<i>T.K. Phuong, L.D. Thuan, and L.H.A. Thuy</i>	
Antifungal Activity of <i>Conyza Canadensis</i> ((L.) Cronquist) Collected in Northern Viet Nam	359
<i>N.B. Phuong, N.T.T. Lien, and N.T.T. Hoai</i>	
Antimicrobial Activity of <i>Senna alata</i> (L.), <i>Rhinacanthus nasutus</i> and <i>Chromolaena odorata</i> (L.) Collected in Southern Vietnam	362
<i>Thuong L.H. Pham, Trung T. Trinh, and Hoai T.T. Nguyen</i>	
Evaluation of the Optimal Multiplex PCR Method for the Detection of <i>Aspergillus Flavus</i> and <i>Aspergillus Parasiticus</i> on Dried Peanut	367
<i>Nghia T. Le, Trinh Huynh, and Hue T. Nguyen</i>	
Evaluation of the Optimal Multiplex PCR Method for the Detection of <i>Aspergillus Flavus</i> and <i>Aspergillus Parasiticus</i> on Dried Corn	371
<i>Tu T. Ly, Trinh Huynh, and Hue T. Nguyen</i>	
fNIRS-Based Wavelet Thresholds for Motor Area Determination	376
<i>Dao.V. Ha, Hai T. Nguyen, Cuong.Q. Ngo, Mai T. Tran, and Toi Van Vo</i>	
Determining the Size of a Solid Tumor	381
<i>Tran Thi Quynh Nhu, Nguyen Thanh Hai, Ngo Thanh Dong, and Nguyen Tan Nhu</i>	
2D Complex Shear Modulus Imaging in Gaussian Noise	385
<i>Nguyen Thi Anh-Dao, Tran Duc-Tan, and Nguyen Linh-Trung</i>	
Evaluation of Frontal and Visual Cortices on Mental Working Tasks Using Functional Near Infrared Spectroscopy	389
<i>Pham Thanh Thao, Nguyen Duc Thang, and Vo Van Toi</i>	
Differentiation of Hemodynamic Responses of the Brain with Typing and Writing	395
<i>Vo Nhut Tuan, Nguyen Duc Thang, Vo Van Toi, Tran Le Giang, Nguyen Huynh Minh Tam, and Dinh Dong Luong</i>	

2D Complex Shear Modulus Imaging in Gaussian Noise

Nguyen Thi Anh-Dao^{1,2}, Tran Duc-Tan², and Nguyen Linh-Trung²

¹ University of Technology and Logistics, Bac Ninh, Vietnam

² Electronics & Telecom., University of Engineering and Technology, Vietnam National University, Hanoi, Vietnam

Abstract— Dynamic shear-wave estimation of complex shear modulus (CSM) has demonstrated the ability to detect tumors. Ultrasound shear wave imaging is one of the methods for quantitatively estimating relevant elasticity parameters of tissues via the wave number and propagation attenuation of ultrasound waves. Maximum Likelihood Ensemble Filter (MLEF) has been efficiently applied for estimating the CSM parameters, but limited to one-dimensional (1D) scenario. This paper extends this method to detecting two-dimensional (2D) objects affected by Gaussian noise during the Doppler acquisition. A ray scanning method is used for modeling the propagation directions (lines) along each of which the MLEF is used for estimating the CSM parameters. The object 2D image is then reconstructed by transforming these estimated CSM parameters from the polar coordinates to Cartesian coordinates. It is not necessary to increase the ensemble size (which means an increase in the algorithm complexity) when the noise level is low.

Keywords— Ultrasound shear wave imaging, maximum likelihood ensemble filter (MLEF), complex shear modulus (CSM), elasticity imaging.

I. INTRODUCTION

Many pathological processes in tissues are recognized by morphological changes that reflect alterations of mechanical properties of soft tissues. Among various elasticity imaging modalities, ultrasonic shear wave imaging technique has been developed for estimating the complex shear modulus (CSM) of biphasic hydro polymers including soft biological tissues. Shear wave imaging has the potential to bridge molecular, cellular and tissue biology, and to support medical diagnoses and patient treatment.

In 2004, Chen et al. found that the propagation speed of shear waves is related to the frequency, the elasticity and viscosity of the medium [1]. Hence, they proposed a method to estimate shear elasticity and viscosity of a homogeneous medium by measuring the shear wave speed dispersion. In 2009, Orescanin et al. applied the Kelvin–Voigt model to estimate the CSM of the liver for shear wave frequencies between 50 and 300 Hz [2]. Then, the Maximum Likelihood Ensemble Filter (MLEF) was applied for CSM estimation for homogeneous medium [3, 4]. It was extended to 1D heterogeneous medium in [5]. In this paper, we extended this

method to detecting two-dimensional objects¹. In addition, we study the effect of Gaussian noise corrupting the Doppler acquisition in conjunction with the effect of the ensemble size of the MLEF.

II. MATERIALS AND METHODS

First, a needle vibrating with the frequency of f (Hz) is used for creating a shear wave whose velocities will then be measured by a Doppler scanner [6]. Second, a ray scanning method is used for modeling the propagation directions. Denote $\alpha(r)$ and $k_s(r)$ the shear wave attenuation coefficient and the wave number at the tracking location r along each ray; r is defined in the polar coordinates as: $r = \rho e^{i\theta}$. Third, the CSM of the tissue located at r is then estimated from $\alpha(r)$ and $k_s(r)$, which are the real and imaginary parts of the CSM value, based on using the Kelvin–Voigt model for a viscous medium [3]. Last, the 2D image of the object is reconstructed by transforming these estimated CSM parameters from the polar coordinates to Cartesian coordinates.

A. Shear Wave Propagation

The needle vibrates along the vertical (z) axis. Under an assumption of cylindrical shear wave propagation along the radial axis, the particle velocity of ray i is a spatio-temporal function of the radial distance r and time t , and is given by

$$v^i(r, t) = \frac{1}{\sqrt{r}} A e^{-\alpha(r)r} \cos(\omega t - k_s(r)r), i = 1, \dots, L \quad (1)$$

where L is number of ray, A is the magnitude of the wave at the source location, ω is the angular shear frequency. In discrete form, we have

$$v_n^i = \frac{1}{\sqrt{r - r_0}} A e^{-\alpha(r)(r - r_0)} \cos(\omega n \Delta t - k_s(r)(r - r_0) - \phi), \quad (2)$$

where index n denotes the discrete time, r_0 is the initial distance from the source, Δt is discrete-time step and ϕ represents the initial temporal phase.

Eq. (2) can be rewritten in a recursive form by:

¹ Part of this study was presented in the 2013 International Conference on Green and Human Information Technology (ICGHIT 2013) as an in-progress work.

$$v_n^i(r) = v_{n-1}^i \cos(\omega \Delta t) - \frac{1}{\sqrt{r-r_0}} A e^{-\alpha(r-r_0)} \times \sin(\omega(n-1)\Delta t - k_s(r-r_0) - \phi) \sin(\omega \Delta t). \quad (3a)$$

Given the effect of Gaussian noise $w_n^i(r)$ on the velocity at each spatial location, we have the following model:

$$v_n^i(r) := v_n^i(r) + w_n^i(r). \quad (3b)$$

B. Attenuation Coefficient and Wave Number Estimation

In this subsection, we apply the MLEF to estimate k_s and α in each ray. The state equation can be constructed from Eq. (3a) as shown below:

$$\mathbf{x} = \begin{bmatrix} \mathbf{v}_n \\ \boldsymbol{\theta}_n \end{bmatrix} = \begin{bmatrix} \mathcal{F}(\mathbf{v}_{n-1}, \boldsymbol{\theta}_{n-1}) \\ \boldsymbol{\theta}_{n-1} \end{bmatrix} \quad (4)$$

where $\boldsymbol{\theta}_n = [\boldsymbol{\alpha}^T, \mathbf{k}_s^T, \phi, r, A]^T$, \mathcal{F} is a nonlinear function modeling the spatial shear wave dynamics. The length of vectors \mathbf{v}_n , $\boldsymbol{\alpha}$ and \mathbf{k}_s equals to the number of spatial locations. We can assume that $\boldsymbol{\theta}_n$ would not be changed during the time of the experiment; hence, $\boldsymbol{\theta}_n = \boldsymbol{\theta}_{n-1}$ as shown in Eq. (4).

By using the Doppler acquisition, the measurements of velocities at every spatial locations are given by

$$\mathbf{y}_n = \begin{bmatrix} \hat{\mathbf{v}}_n \\ \mathbf{0} \end{bmatrix} = [\mathbf{I} \quad \mathbf{0}] \begin{bmatrix} \mathbf{v}_n \\ \boldsymbol{\theta}_n \end{bmatrix} + \begin{bmatrix} \mathbf{w} \\ \mathbf{0} \end{bmatrix}, \quad (5)$$

where \mathbf{w} is the measurement noise vector.

From Eqs. (4) and (5), the shear wave attenuation coefficient $\alpha(r)$ and the wave number $k_s(r)$ of each ray are estimated by using MLEF according to the algorithm in [4].

C. CSM Estimation Using Kelvin-Voigt Rheological Model

We apply the Kelvin-Voigt model, as illustrated in Fig.1, to estimate the CSM. For a viscous elastic medium, the CSM μ is modeled by an elastic component μ_1 in parallel with the dynamic viscous component η as:

$$\boldsymbol{\mu} = \bar{\boldsymbol{\mu}} - i\omega\boldsymbol{\eta}, \quad (6)$$

The complex wave number for a viscous medium is given by

$$k_s' = \sqrt{\rho\omega^2/\boldsymbol{\mu}}. \quad (7)$$

Since k_s' is complex, it can be written as

$$k_s' = k_s - i\alpha, \quad (8)$$

From (7) and (8), by estimating k_s and α , we can obtain μ .

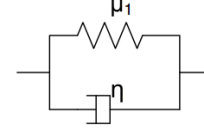


Fig. 1 Diagram of Kelvin-Voigt model

D. Detecting the Presence of 2 D Object

In this work, we verify the proposed method using a two-object simulation scenario. Each object was ‘placed’ at a certain spatial location $r = \rho e^{i\theta}$. We use a ‘ray scanning’ method to cover the area of interest, in steps of a constant angle (see Fig. 2). The whole area is scanned by varying θ from 0° to 90° in step of 1° , creating 90 rays of interest. Given the availability of 43 elements in the in-use Doppler scanner, we select 43 evenly-spaced spatial locations r along each ray. After collecting all information of these 90 rays, we estimated $\alpha(r)$ and $k_s(r)$. For a given CSM value μ corresponding to a particular material of an object under interest, we establish a detection threshold pair of (α^*, k_s^*) such that the object is detected to be present if the following conditions: $\alpha(r) > \alpha^*$ and $k_s(r) < k_s^*$ for all r . In this paper, the value of the threshold pair can be found empirically via numerical simulation.

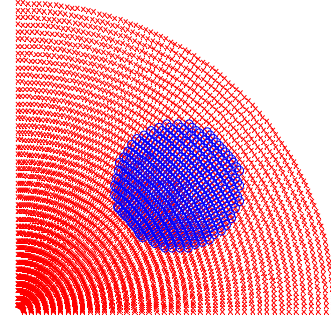


Fig. 2 Ray scanning illustration

III. NUMERICAL RESULTS AND DISCUSSIONS

In this study, we examine the proposed method for detecting 2 circular objects whose elasticity properties are different (i.e., the CSM values are different). Object 1 is placed at location (6 mm, 1.4 mm) with the radius of 1.4 mm. Object 2 is placed at (10 mm, 8 mm) with the radius of 3 mm. The CSM values of the two objects are $(\bar{\mu} = 900 \text{ Pa}, \eta = 0.3 \text{ Pa/s})$ and $(\bar{\mu} = 800 \text{ Pa}, \eta = 0.2 \text{ Pa/s})$ respectively. Accordingly, we have $(\alpha = 67.5; k_s = 651.7)$ for Object 1 and $(\alpha = 54.3; k_s = 696)$ for Object 2. We assume that the first spatial location, r_0 , is close to the needle: $r_0 = 0.4 \text{ mm}$.

Base on empirical study, we found that the detection threshold pair for Objects 1 and 2 are $(\alpha^* = 50; k_s^* = 670)$ and $(\alpha^* = 44; k_s^* = 710)$, respectively. The amplitude A and the phase ϕ are estimated using the first cycle of the particle velocity at r_0 . These parameters are then used for calculating the initial state vector of the MLEF. The initial error square-root covariance matrix is Gaussianly randomly generated. After only tens of iterations, the velocity is denoised and the attenuation and wave number are estimated. Based on the results obtained from the MLEF, we apply Kelvin – Voigt rheological model to estimate CSM. Finally, we construct the 2D image. The 2D image in Cartesian coordinates of the simulation scenario is shown in Fig. 3.

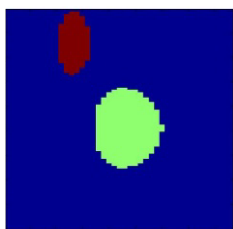


Fig. 3 Original image.

A. In Noise-Free Environment

Fig. 4 shows the estimated $\alpha(r)$ and $k_s(r)$ from rays 4 and 45, which are chosen specifically so that ray 4 passes Object 1 and ray 45 passes Object 2, with no noise effect in the Doppler acquisition. The solid curves are the estimated attenuation and wave number, and the dashed curves are ideal ones. It is shown that Object 1 is detected to be present in the interval of $r = [11, 16]$ and Object 2 in that of $r = [18, 30]$. In this study, the MLEF ensemble size is $s = 86$, which is equal to twice the number of elements of the Doppler scanner.

Then, the 2D reconstructed image and their 2D images of attenuation and wave number are shown in Fig. 5. It is obvious that the objects were detected. However, it can be seen that the wave number was better estimated than the attenuation.

B. In Gaussian Environment

Figures 6 to 9 illustrate the effect of Gaussian noise and the MLEF ensemble size on the reconstructed images and their corresponding images of attenuation and wave number, tested for the signal-to-noise ratio (SNR) of 40 and 34 dB and the ensemble size of 43 and 86. With a large value of the ensemble size ($s = 86$), we were able to detect the objects when the Doppler acquisition was corrupted by the noise.

Fig. 10 provides an insight into the effect of the ensemble size on the image reconstruction, measured by the peak-signal-to-noise ratio (PSNR), with respect to different noise levels (SNR = 20 to 40 dB). It can be seen that at a high-level of noise, a higher ensemble size offers a larger PSNR, which means a better quality. However, it is not necessary to increase the ensemble size (which means an increase in the algorithm complexity) when the noise level is low.

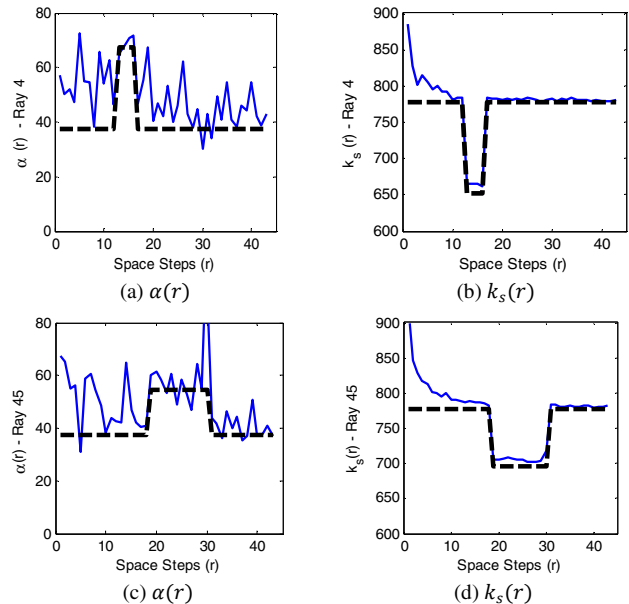


Fig. 4 $\alpha(r)$ and $k_s(r)$ along ray 4 (top) and ray 45 (bottom); $s = 86$.

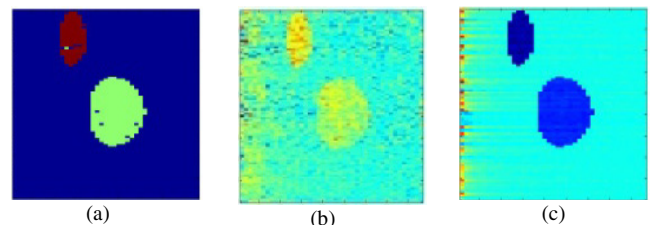


Fig. 5 Reconstructed image (a), Attenuation (b) Wave number (c) images with ensemble size of $s = 86$.

IV. CONCLUSIONS

Based on the MLEF approach, this paper has proposed a ray-tracing based method to estimate the elasticity properties of 2D objects in shear wave imaging. The experiment is quite simple when only a single vibration frequency is needed to accurately estimate the CSM in the medium. Quantitative analysis for different levels of Gaussian noise affecting the Doppler acquisition, the ensemble size were studied. In future work, it is desirable to examine further

thoroughly the optimal imaging thresholds pair, (α^*, k_s^*) , used for detecting the objects under various practical CSM values. In addition, better estimation of the attenuation should be investigated.

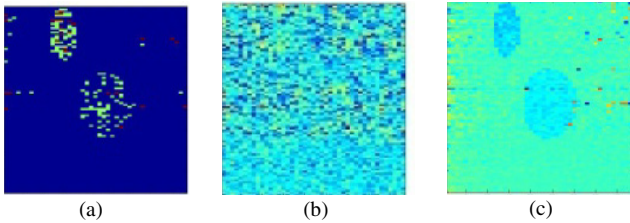


Fig. 6 Reconstructed (a), Attenuation (b), and Wave number images with $s = 43$, SNR = 40 dB. The obtained PSNR = 10.4.

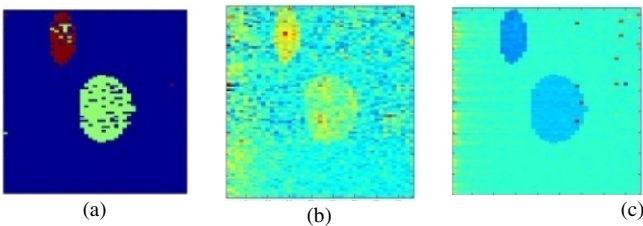


Fig. 7 Reconstructed (a), Shear attenuation (b), and Wave number images with $s = 86$, SNR = 40 dB. The obtained PSNR = 10.31.

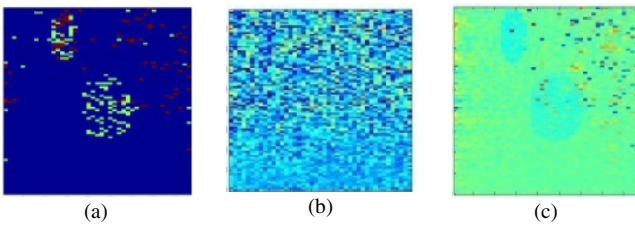


Fig. 8 Reconstructed (a), Shear attenuation (b), and Wave number images with $s = 43$, SNR = 34 dB. The obtained PSNR = 6.58.

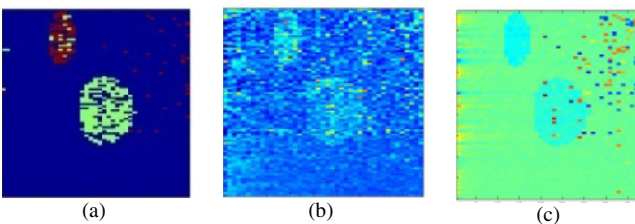


Fig. 9 (a) Reconstructed (a), Shear attenuation (b), and Wave number images with $s = 86$, SNR = 34 dB. The obtained PSNR = 8.46.

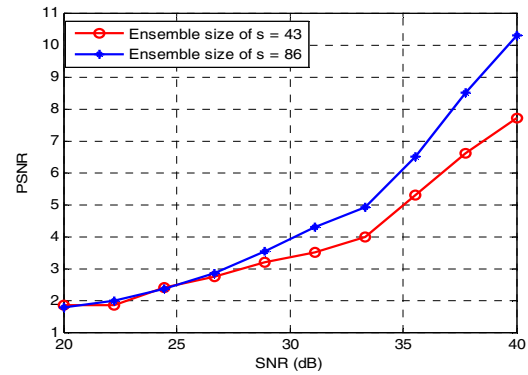


Fig. 10 Effects of noise and ensemble size.

REFERENCES

1. Chen, S et al.: Quantifying elasticity and viscosity from measurement of shear wave speed dispersion. *Journal of Acoustic Soc Am.* 115, 2781-2785 (2004).
2. Marko Orescanin, et al.: Complex Shear Modulus of Thermally-Damaged Liver, pp127 – 130. *Ultrasonics Symposium (IUS), 2009 IEEE International.*
3. Orescanin, M. et al.: Model-based complex shear modulus reconstruction: A Bayesian approach. In: *IEEE Int'l Ultrasonics Symposium*, pp. 61-64. IEEE Press (2010).
4. Zupanski, M.: Maximum Likelihood Ensemble Filter: Theoretical Aspects. *Monthly Weather Review.* 133, 1710-1726 (2005).
5. Tan Tran-Duc, et al.: Complex shear modulus estimation using the maximum likelihood ensemble filter, *BME'04*, 2012.
6. Orescanin et al.: Shear Modulus Estimation With Vibrating With Needle Stimulation. *IEEE Trans. Ultrasonics, Ferroelectrics, and Frequency Control.* 57, 1358-1367 (2010).

Author: Nguyen Thi Anh-Dao
 Institute: University of Technology and Logistics
 Street: Ho town, Thuan Thanh district
 City: Bac Ninh
 Country: Viet Nam
 Email: daonta81@gmail.com